DOI: 10.1002/ejic.200700644

# Order-Disorder Phase Transition in Type-I Clathrate $Cs_8Sn_{44}\square_2$

**Andreas Kaltzoglou,[a] Stephan D. Hoffmann,[a] and Thomas F. Fässler*[a]**

*Dedicated to Prof. Dr. G. Huttner on the occasion of his 70th birthday*

**Keywords:** Clathrates / Order-disorder transitions / Single-crystal structure analysis / Thermoelectricity / Tin

The clathrate compound α-$Cs_8Sn_{44}\square_2$ has been synthesized from its elements under inert gas conditions and has been characterized by single-crystal and powder X-ray diffraction. At room temperature, it crystallizes with cubic symmetry [$a$ = 24.256(3) Å, space group $Ia\bar{3}d$, $Z$ = 8] and adopts a $2\times2\times2$ superstructure of the type-I clathrate and a high ordering of the vacancies (□) in the Sn framework. Single crystals of α-$Cs_8Sn_{44}\square_2$ reversibly transform at 90 °C to the high-temperature β form with primitive symmetry [$a$ = 12.135(1) Å, space group $Pm\bar{3}n$, $Z$ = 1] and a lower ordering of the defects. Differential thermal analysis corroborates the reversible character of the phase transition, which occurs with an enthalpy change of approximately 0.38 $J\,g^{-1}$. An atom-migration mechanism describing the order-disorder transition involving spiro-connected six-membered rings only (scsr mechanism) is proposed.


## Introduction

The discovery of clathrates as a distinct class of materials opened up a wide area of research involving specifically further synthesis and studies of their properties. The binary systems composed primarily of alkali or alkaline earth metals as guests and Group 14 elements (Si, Ge, Sn) as hosts of the three-dimensional framework are known as semiconducting clathrates and behave mostly like Zintl phases rather than typical intermetallic compounds.[1] The idea that clathrate compounds fulfill the criteria for the Phonon Glass Electron Crystal (PGEC) concept[2] and thus may qualify as thermoelectric materials has led to the rapid development of this compound family. Over the last decades, five clathrate structure types denoted with the Latin numbers I, II, III, VIII, IX have been established, with type I as the most common (Figure 1). In clathrate I, the tetravalent host atoms form interconnected polyhedra with shared pentagonal and hexagonal faces. The structure is further stabilized in the presence of the encaged metal cations. Even though much data on the composition, crystal structures, and physical properties are now available,[3–5] there is still a lack of understanding of the physics involved in the PGEC approach. A strong glass-like rattling of the guest atoms inside the cages of the three-dimensional network of host atoms is necessary for achieving high-quality thermoelectric materials. Therefore, a fine grasp of the lattice defects and phase transitions in clathrate-I compounds must play a decisive role in the understanding of the structure–property relationships in stannide clathrates.

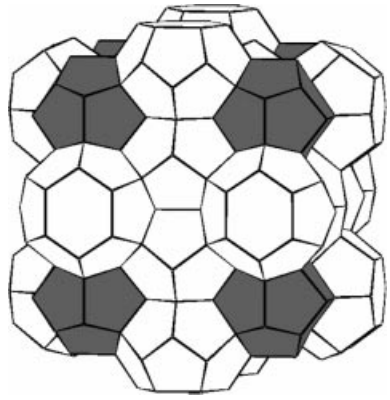

Figure 1. Structure of the type-I clathrate with pentagonal dodecahedra (grey [$5^{12}$]) and tetrakaidecahedra (white [$5^{12}6^2$]) in a 1:3 ratio.

A limited number of such compounds undergo phase transitions before melting. Interestingly, those temperature- or pressure-induced structural transformations can also affect certain physical properties. Recently, a magnetocaloric effect was reported for the doped $Eu_8Ga_{16}Ge_{30}$ resulting from the ferromagnetic transition from a type-I to a type-VIII structure.[6] Moreover, type-IX $Ba_6Ge_{25}$[7] tunes its electrical properties through a two-step phase transition, and phonon band structures of the non-defect type-I $K_8Si_{46}$ change drastically upon pressing.[8]

[a] Department of Chemistry, Technische Universität München, Lichtenbergstr. 4, 85747 Garching, Germany
E-mail: thomas.faessler@lrz.tum.de
Supporting information for this article is available on the WWW under http://www.eurjic.org or from the author.

Since the first report of the non-defect $K_8Sn_{46}$,[9] the exact composition and structure of the type-I tin clathrates was brought into question several times.[10,11] The discrepancies involve the presence of defects – a prerequisite for fulfilling the Zintl–Klemm concept – and their ordering in the crystal. A Mulliken population analysis[12] on the basis of topological charge stabilization for the stannides showed that the vacancies in the three-dimensional host lattice of Sn atoms are favored and that they are statistically distributed only at the framework sites that are part of six-membered rings and that do not belong to pentagonal dodecahedra (6 out of 46 sites); those possess the lowest electron density. These assumptions were indeed confirmed experimentally as the $A_8Sn_{44}\square_2$ compounds (A = K, Rb, Cs)[4,5,13] were found to crystallize in the $Pm\bar{3}n$ space group and the partially occupied positions were distributed along a $4_2$ screw axis. More recently, theoretical calculations for $Cs_8Sn_{44}$[14] and $K_8Sn_{44}$[15] indicated that one vacancy per six-membered ring is favored over two such vacancies per ring. A superstructure was experimentally established for $Rb_8Sn_{44}\square_2$, which was found to crystallize in the $Ia\bar{3}d$ space group and the $2\times2\times2$ unit cell with vacancies distributed along a $4_1$ axis instead of the $4_2$ axis (see also Figure 2).[16] However, the conditions under which the two modifications occur, or if they may co-exist, still remained unclear.

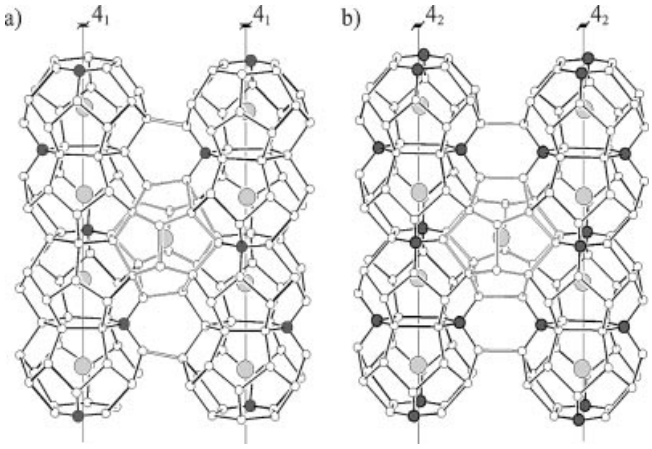


Figure 2. Partial view of the $Cs_8Sn_{44}\square_2$ structures composed of two chains of tetrakaidecahedra and one pentagonal dodecahedron. a) In the α form (space group $Ia\bar{3}d$), the partially occupied *24c* sites (dark grey Sn6 atoms, with an occupation factor of 0.339) are distributed along a $4_1$ helical axis. b) In the β form (space group $Pm\bar{3}n$), the partially occupied *6c* sites (dark grey Sn1 atoms, with an occupation factor of 0.687) are distributed along a $4_2$ axis. In both cases, only the Sn atoms of the split positions with closer contacts to the vacancy are shown.

Here we report on the discovery of a reversible phase transition of isostructural $Cs_8Sn_{44}\square_2$. The transformation sheds light on the structural trends of defect tin clathrates. Since we expect that most stannide clathrate-I compounds appear at low temperatures with a $2\times2\times2$ superstructure, the partial ordering of vacancies must be considered on the basis of property measurements and this might lead to a reinterpretation of several studies.[5,17]

## Results and Discussion

According to the room temperature powder X-ray analysis, $Cs_8Sn_{44}\square_2$ adopts the type-I clathrate structure with a superstructure as observed for $Rb_8Sn_{44}\square_2$.[16] The cell parameters and the space group [$a$ = 24.256(3) Å, space group $Ia\bar{3}d$] are confirmed by single-crystal analysis at room temperature. The single crystal of $Cs_8Sn_{44}\square_2$ was gradually heated on the diffractometer with steps of 20 °C. No significant changes in the reflection patterns occur until a temperature of 80 °C was reached. At 100 °C, the superstructure reflections of the low temperature form (α-$Cs_8Sn_{44}\square_2$) disappear (see Supporting Information) as the crystal transforms into the primitive lattice with smaller cell parameters. This has been observed previously for $Cs_8Sn_{44}$ (β form).[13] A full data set was collected at this temperature. The crystal was perfectly retained when cooled at a rate of 2 °C min$^{-1}$ to room temperature where a second set of data was collected, which confirmed the full reversibility of the phase transformation.

At 20 °C, the $Cs_8Sn_{44}\square_2$ clathrate crystallizes in the $Ia\bar{3}d$ centrosymmetric space group (Figure 2a). The partially occupied Sn6 sites of the polyanionic framework [Wyckoff position *24c*, occupation factor 0.339(6)] are distributed around a $4_1$ screw axis through the Cs atoms that reside in the tetrakaidecahedra. As a consequence, a split model for the adjacent *96h* site is adopted, which gives rise to Sn4a atoms [occupation factor 0.339(6)] and Sn5b atoms [occupation factor 0.661(6)] that correspond to occupied and vacant Sn6 sites, respectively. Further, the Sn3 atom has a relatively large $U_{eq}$ value [0.0263(3) Å$^2$], probably because three out of its four neighbors are the split Sn4a/Sn4b atoms (Table 1). Nevertheless, no split model could be applied for this position. Further, two crystallographically non-equivalent positions for the Cs atoms are observed: (i) The Cs1 atom located in the dodecahedra and (ii) The Cs2 atom located in the tetrakaidecahedra. In both cases the sites are fully occupied. The isotropic atomic displacement parameters are 0.0193(3) Å$^2$ and 0.0378(2) Å$^2$ for Cs1 and Cs2, respectively, proving the stronger "rattling" of the guest in the larger cavities. It is also worth mentioning that the Cs2 atoms do not reside exactly in the center of the cavities, but tend to the opposite site of the vacancy, namely closer to the Sn5 atom (*24d* Wyckoff position). Thus, a slight deviation from linearity (178.88°) is observed for the

Table 1. Atomic coordinates and equivalent isotropic displacement parameters for α-$Cs_8Sn_{44}\square_2$.

| Atom | Site | $x$ | $y$ | $z$ | Occupancy | $U_{eq}$ [Å$^2$] |
|---|---|---|---|---|---|---|
| Cs1 | *16a* | 0.5000 | 0.5000 | 0.0000 | 1 | 0.0193(3) |
| Cs2 | *48g* | 0.6250 | 0.24827(3) | 0.00173(3) | 1 | 0.0378(2) |
| Sn1 | *96h* | 0.50096(3) | 0.34668(2) | 0.05598(2) | 1 | 0.0170(2) |
| Sn2 | *96h* | 0.59456(3) | 0.40950(3) | 0.08969(3) | 1 | 0.0179(2) |
| Sn3 | *32e* | 0.59130(3) | 0.40870(3) | –0.09130(3) | 1 | 0.0263(3) |
| Sn4a | *96h* | 0.5029(2) | 0.3487(2) | –0.0599(2) | 0.339(6) | 0.0167(7) |
| Sn4b | *96h* | 0.5011(1) | 0.3275(1) | –0.06679(9) | 0.661(6) | 0.0185(4) |
| Sn5 | *24d* | 0.5000 | 0.2500 | 0.1250 | 1 | 0.0145(3) |
| Sn6 | *24c* | 0.5000 | 0.2500 | –0.1250 | 0.339(6) | 0.016(1) |

  

Cs2–Cs2–Cs2 chain parallel to the cubic axes, which is expressed in terms of displacement of 0.0593 Å from the center of the cage.

In the high temperature modification (space group $Pm\bar{3}n$), the *6c* Wyckoff site corresponds to the Sn1 atom with occupation factor 0.687(7) (Table 2). Within the standard deviation, this value is equivalent to the value of the I-centered crystals at room temperature and to the value of 2/3, anticipated for an electron precise Zintl phase. As expected, the adjacent *24k* site is better refined by means of a Sn3a/Sn3b model with occupancies 0.687(7) and 0.313(7), respectively. Once again, the Cs atoms that reside in the large framework cavities exhibit much higher atomic displacement parameters than those in the smaller cavities. The β modification exhibits larger ADPs (ADP = anisotropic displacement parameter) than the α modification and the values obtained from the room temperature data refinement in ref.[13], as expected from the temperature dependence in the Einstein's oscillator model.[5a] On the other hand, the Sn–Sn–Sn angles have very comparable values: 94.84(7)°–126.52(9)° for the I lattice and 94.68(1)°–125.2(1)° for the primitive lattice.

Table 2. Atomic coordinates and equivalent isotropic displacement parameters for β-$Cs_8Sn_{44}\square_2$.

| Atom | Site | *x* | *y* | *z* | Occupancy | $U_{eq}$ [Å$^2$] |
|---|---|---|---|---|---|---|
| Cs1 | *2a* | 0.0000 | 0.0000 | 0.0000 | 1 | 0.0223(5) |
| Cs2 | *6d* | 0.2500 | 0.5000 | 0.0000 | 1 | 0.0478(6) |
| Sn1 | *6c* | 0.2500 | 0.0000 | 0.5000 | 0.687(7) | 0.0197(9) |
| Sn2 | *16i* | 0.18314(4) | 0.18314(4) | 0.18314(4) | 1 | 0.0259(3) |
| Sn3a | *24k* | 0.0000 | 0.3064(2) | 0.1136(3) | 0.687(7) | 0.0233(5) |
| Sn3b | *24k* | 0.0000 | 0.3447(6) | 0.1344(6) | 0.313(7) | 0.025(1) |

The structure of α-$Cs_8Sn_{44}$ was verified by Rietveld refinement of the powder diffraction pattern. In this case as well, split models for the positions adjacent to the vacancies are applied.

The vacancy order–disorder transformation is also detectable by differential thermal analysis (DTA). At about 95 °C, a weak endothermic peak, which can be attributed to the $Ia\bar{3}d \rightarrow Pm\bar{3}n$ transition is observed (Figure 3). The reverse phenomenon takes place and is observed as an exothermic peak during cooling. The hysteresis of the peaks depends on the heating and cooling rate. From the average of the experimental maxima, one can define the transition temperature at $T_t$ = 89–90 °C. Further heating to 1000 °C at a rate of 10 °C min$^{-1}$ results in an endothermic peak at 580 °C (on set), which according to the phase diagram is attributed to peritectical decomposition of $Cs_8Sn_{44}$ into Sn and $CsSn_2$.[18] Finally, at 830 °C, a relatively weak and broad endothermic peak of the liquidus line is observed. On cooling, each peak has a corresponding exothermic phenomenon at 810 °C, 510 °C, and 215 °C, which corresponds to the solidification of Sn. Elemental Sn was initially not observed in the room temperature X-ray powder diffractogram. However, it has been shown by multitemperature diffraction experiments with synchrotron X-rays that the related compound $Rb_8Sn_{44}$ contains small amounts of impurities. The impurities are formed as a decomposition product already at 180 °C.[19] The X-ray powder diffraction pattern of the DTA residue after heating to 1000 °C was refined by the Rietveld method. It confirms the presence of α-$Cs_8Sn_{44}$ with a lower degree of crystallinity and also the formation of β-Sn, to approximately 6%.

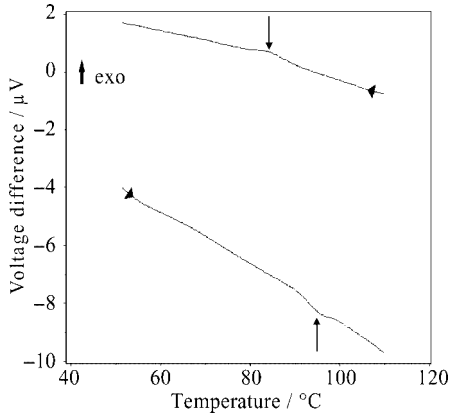


Figure 3. Section of the DTA diagram of $Cs_8Sn_{44}\square_2$ recorded in the range 25 °C–150 °C at a 1 °C min$^{-1}$ heating and cooling rate. Shown is the section between 50 °C and 110 °C. Vertical arrows show the endothermic and exothermic peaks.

The recent observation of a superstructure for clathrate-I $Rb_8Sn_{44}$[16] raises the question on the one hand if such an ordering of vacancies occurs in other stannides with clathrate-I structures and on the other hand why this superstructure has not been observed although many reports on those structures have been published. The detailed thermal analysis here shows that the phase transformation occurs at 89–90 °C with almost perfect reversibility. On the basis of the on set temperatures on heating and cooling the sample at 1 °C min$^{-1}$, the transition occurs with a hysteresis of approximately 2°. Even quenching of the reaction product from 100 °C or 700 °C into liquid nitrogen did not give rise to the high temperature β modification. During all transformations, no other impurity than small amounts of β-Sn was detected by X-ray powder diffraction, EDX, or DTA.

In general, superlattice formation can prevent under- or mixed occupancy of specific atomic sites, but can achieve vacancy formation and atom segregation. Four examples of superstructures have been discussed for doped and/or defect type-I clathrates: (a) $I_8[Sn_{14}In_{10}P_{21.2}\square_{0.8}]$ crystallizes in the tetragonal space group $P4_2/m$, exhibiting partial ordering of the defects;[20] (b) the orthorhombic (*Pbcn*) $Ba_8[Cu_{16}P_{30}]$ exhibits no disorder as P atoms exclusively occupy the *24k* and *6c* sites and Cu atoms the *16i* sites;[21] (c) more recently, the cubic ($Ia\bar{3}d$) $Rb_8Sn_{44}\square_2$ shows a partial ordering of the vacancies;[16] (d) $Ba_8Ge_{43}\square_3$ is characterized as a fully ordered superstructure when quenched quickly from 800 °C or as partially ordered when cooled slowly to ambient conditions.[22] In the present case as in $Rb_8Sn_{44}\square_2$ and $Ba_8Ge_{43}\square_3$, a "klassengleiche" symmetry reduction from

  

*Pm*$\bar{3}$*n* to *Ia*$\bar{3}$*d* takes places. However, the absence of a distinct transition temperature and the higher thermodynamic stability of the disordered modification for $Ba_8Ge_{43}\square_3$ are in contrast to our results here. For $Cs_8Sn_{44}\square_2$, as expected, the model with a lower degree of atom ordering represents the high temperature modification.

The full ordering of the defects in $Ba_8Ge_{43}\square_3$ is also reflected in the larger deviation of the position of the guest atom Ba from the ideal center of the tetrakaidecahedra. The larger displacement of the Ba atoms (0.0844 Å) originates from the presence of a full vacancy and not from the statistics of a partially filled position, as found in $Cs_8Sn_{44}\square_2$ with a displacement of 0.0593 Å for Cs.

According to DTA experiments, the phase transition occurs well below the melting temperature and involves an enthalpy change of about $\Delta H_t = -0.38\ J\,g^{-1}$ ($-2.390\ kJ\,mol^{-1}$) and is thus lower in energy than the first-order transition α-Sn → β-Sn at 13.2 °C ($\Delta H_t = -17.6\ J\,g^{-1}$ or $-2.089\ kJ\,mol^{-1}$).[23] Perfect preservation of the single crystal during the phase transition suggests a second-order transition. However, the enthalpy change at a distinct transition temperature shows that first-order contributions must also be considered.

We rationalize the different thermodynamic stability of the two modifications by studying the possible configurations of the hexagons in $[5^{12}6^2]$. In α-$Cs_8Sn_{44}\square_2$, each hexagon may either be defect-free or possess one defect. In the latter case the neighboring atomic positions are shifted towards the vacancy (Figure 4). In β-$Cs_8Sn_{44}\square_2$, in addition to the two configurations in Figure 4 with virtually identical structures, a third configuration with two vacancies per hexagon in the *para* positions may also occur (Figure 5). Consequently, the bonds between the remaining four atoms are even more elongated, i.e. 3.26(1) Å, which is about 0.3 Å longer than typical distances between three-bonded Sn atoms [see for example the tetrahedral $Sn_4$ clusters in $Cs_4Sn_4$ in which Sn–Sn = 2.939(2) Å].[24]

This next-nearest neighbor interaction of two vacancies significantly affects the stability of the system. Local density approximation studies on the hypothetical $Cs@Sn_{22}\square_2$ with isolated 24-atom cages show that the situation with the vacancies on two different six-membered rings is favored over that in which both vacancies are on the same ring.[14] These theoretical results reflect the trend obtained here experimentally, i.e. vacancy ordering is favored at room temperature. Despite the low enthalpy, no equilibrium is observed between the two modifications, as is also indicated by the first-order contribution to the phase transformation. On the other hand, β-$Cs_8Sn_{44}\square_2$ possesses higher symmetry than α-$Cs_8Sn_{44}\square_2$. For this reason and despite the thermodynamic instability, the disordered modification is favored at elevated temperatures by means of an entropy-driven phase transition.

The mechanism of this low-energy enantiotropic solid-state transformation can be rationalized as a continuous path rather than a nucleation-and-growth process that begins at the imperfections of the crystal.[25] Two ways of achieving the migration of certain Sn atoms are proposed

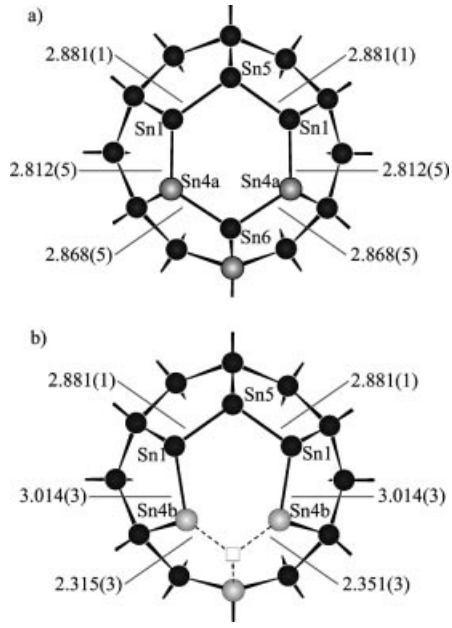


Figure 4. Perpendicular view of a hexagon in α-$Cs_8Sn_{44}\square_2$: a) no defects, b) one defect. All distances are given in Å.

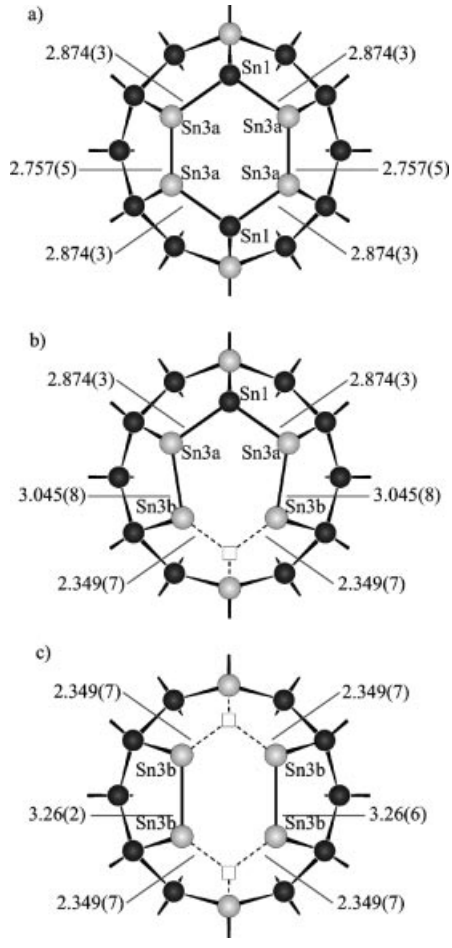


Figure 5. Perpendicular view of a hexagon in β-$Cs_8Sn_{44}\square_2$: a) no defects, b) one defect, c) two defects. All distances are given in Å.

  

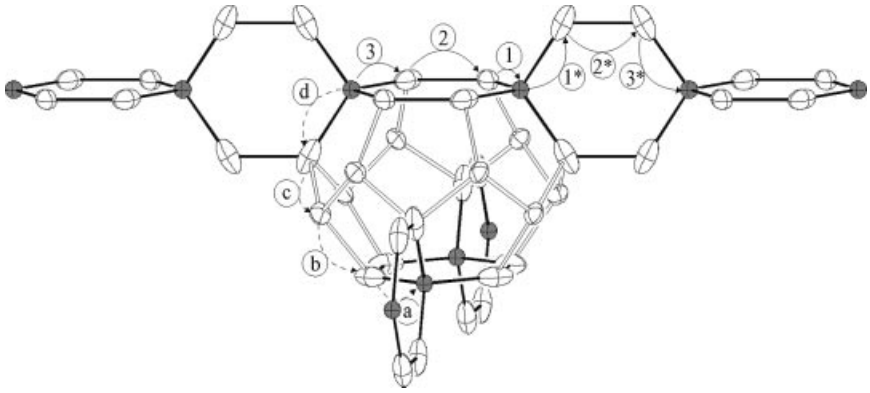


Figure 6. Two possible mechanisms of atom migration for the $Pm\bar{3}n$ to $Ia\bar{3}d$ phase transition. Fully and partially occupied Sn positions are drawn in white and grey, respectively, with thermal ellipsoids at the 80% probability level and without split positions for atoms adjacent to the vacancies.

(Figure 6): (a) A three-step mechanism including migration via two split positions within a six-membered ring is indicated as solid arrows. Migration occurs along spiro-connected six-membered rings (scsr) only. Because of the cubic symmetry, the spiro motive shown in Figure 6 appears in chains along all three directions and allows the rearrangement of the atoms in the three-dimensional framework. (b) A four-step mechanism with migration through two split and one non-split atomic positions, the latter being part of five-membered rings only, is indicated as dashed arrows. Large displacement vectors of the involved atoms favor the scsr mechanism.

## Conclusions

The present study establishes the temperature-dependent phase transition of $Cs_8Sn_{44}$ and sheds light on the controversial discussion of the properties of clathrate-I stannides. Still a question remains: could a fully ordered structure with the composition of an electron-precise Zintl phase $A_8Sn_{44}\square_2$ exist? The full ordering could occur in an enlarged $6\times6\times6$ unit cell with space group $Ia\bar{3}d$ or alternatively in a $3\times3\times3$ unit cell with $Pm\bar{3}n$ symmetry.[26] Nevertheless, no such superlattices were found by single-crystal analysis above –130 °C.

## Experimental Section

**Synthesis:** The $Cs_8Sn_{44}\square_2$ clathrate was prepared from the pure elements, which were handled in an Ar-filled glove box ($O_2$ and $H_2O$ levels <0.1 ppm). Stoichiometric amounts of Cs (ampoule, >98%, Riedel de Haën) and Sn (granules, 99.999%, Chempur) were weighted into Nb ampoules and sealed under reduced Ar pressure. The crucibles were subsequently closed in evacuated silica tubes (pressure ca. $3\times10^{-2}$ mbar), heated to 750 °C for 12 h (2 °C min$^{-1}$), slowly cooled to 500 °C (0.1 °C min$^{-1}$), held at this temperature for 10 d, and then air-quenched to ambient temperature. The title compound exhibits air and moisture stability and remains unchanged upon standing for months. Variation of the reactions conditions, such as reaction temperature between 700 °C and 950 °C, annealing steps, and cooling rates from 0.1 °C min$^{-1}$ to air-quenching, did not significantly affect the composition of the product; however, the quality of the crystals were affected and β-Sn disappeared by increasing the annealing times.

**X-ray Powder Diffraction:** The air-stable and metal-like products were identified on a STOE STADI powder diffractometer equipped with a linear position sensitive detector, using Cu-$K_\alpha$ radiation ($\lambda$ = 1.5406 Å, $10° \le 2\theta \le 90°$, step width = 0.01°) in transmission mode. Microcrystalline diamond was used as the internal standard. The patterns were indexed by using the software package WinXPOW (Stoe) and refined with the WinPLOTR program.[27]

**Single-Crystal X-ray Diffraction:** Reflection data sets were collected with a Stoe IPDS-IIT image plate diffractometer with graphite monochromated Mo-$K_\alpha$ radiation ($\lambda$ = 0.71073 Å) and an open-flow $N_2$ blower for the temperature range –180 °C to 100 °C (Oxford Cryostream Cooler). The temperature at the crystal was additionally checked at various heating steps by using an external thermocouple. Good quality single crystals were obtained by annealing the samples at 400–500 °C for several days. One plate-like crystal was transferred into a glass capillary (Hilgenberg, length = 80 mm, diameter = 0.3 mm) that were in turn mounted on the diffractometer. After checking the cell parameters and the space group ($a$ = 24.256 Å, $Ia\bar{3}d$), the crystal was subsequently heated to 100 °C. Data sets were collected at 100 °C with $a$ = 12.135 Å and the space group $Pm\bar{3}n$ and after cooling to 20 °C with $a$ = 24.256 Å and the space group $Ia\bar{3}d$ (Table 3). For structure solutions and refinements (direct methods, full-matrix least-squares on $F^2$, anisotropic atomic displacement parameters for all atoms, with numerical absorption corrections[28]), SHELXTL97 was used.[29] Note also that the occupation factors for defects and split positions were coupled through the PART command for disordered groups. Further details of the crystal structure investigations can be obtained from the Fachinformationszentrum Karlsruhe, 76344 Eggenstein-Leopoldshafen, Germany [Fax: (+49)7247-808-666; E-mail: crysdata@fiz-karlsruhe.de] on quoting the depository numbers CSD-417969 (α form) and 417970 (β form).

**Differential Thermal Analysis:** DTA was carried out on an annealed sample ($m$ = 370 mg) sealed in an Nb-crucible under an argon, protective atmosphere in the temperature range 25–1000 °C. The diagrams were obtained in two cycles using heating and cooling rates from 0.1 to 5 °C min$^{-1}$. The calibration was carried out by using known latent heats for the melting points of naphthalene ($T_m$ = 80.3 °C, $\Delta H_m$ = –147 J g$^{-1}$), In ($T_m$ = 156.6 °C, $\Delta H_m$ = –28.6 J g$^{-1}$), β-Sn ($T_m$ = 231.9 °C, $\Delta H_m$ = –60.5 J g$^{-1}$), and Al ($T_m$ = 660.3 °C, $\Delta H_m$ = –397 J g$^{-1}$) at a rate of ±2 K min$^{-1}$. The latent

  

Table 3. Crystal and structure refinement data for β-$Cs_8Sn_{44}\square_2$ (high temperature form) and α-$Cs_8Sn_{44}\square_2$ (low temperature form).

| | | |
|---|---|---|
| Chemical formula | β-$Cs_8Sn_{44.12(3)}$ | α-$Cs_8Sn_{44.02(1)}$[a] |
| Space group (No.) | $Pm\bar{3}n$ (223) | $Ia\bar{3}d$ (230) |
| Formula weight | 6299.88 | 6287.53 |
| Temperature, $T$ [°C] | 100 | 20 |
| Radiation, $\lambda$ [Å] | Mo-$K_\alpha$, 0.71073 | Mo-$K_\alpha$, 0.71073 |
| $Z$ | 1 | 8 |
| $\rho_{calcd.}$ [g cm$^{-3}$] | 5.840 | 5.851 |
| $A$ [Å] | 12.135(1) | 24.256(3) |
| $V$ [Å$^3$] | 1787.1(4) | 14272(3) |
| Absorption coeff., $\mu$ [mm$^{-1}$] | 19.06 | 19.10 |
| F (000) | 2640 | 21120 |
| $\theta$ range for data collection [°] | 4.11–25.24 | 2.06–25.25 |
| Index ranges | $0 \le h \le 8$, $0 \le k \le 10$, $2 \le l \le 14$ | $0 \le h \le 16$, $0 \le k \le 20$, $2 \le l \le 29$ |
| Reflections collected | 27209 | 85339 |
| Independent reflections | 317 ($R_{int}$ = 0.108) | 1083 ($R_{int}$ = 0.085) |
| Parameters | 23 | 53 |
| Goodness-of-fit on $F^2$ | 0.815[b] | 1.065[c] |
| Final $R$ indices [$I > 2\sigma(I)$] | $R_1$ = 0.020, $wR_2$ = 0.042 | $R_1$ = 0.035, $wR_2$ = 0.054 |
| $R$ indices (all data) | $R_1$ = 0.035, $wR_2$ = 0.043 | $R_1$ = 0.054, $wR_2$ = 0.058 |
| Largest diff. peak and hole [e Å$^{-3}$] | 0.678 and –1.308 | 0.775 and –1.185 |

[a] Data collection after heating the single crystal to 100 °C. [b] Final weighting scheme = $1/[\sigma^2(F_o^2) + (0.0232P)^2]$ where $P = (F_o^2 + 2F_c^2)/3$. [c] Final weighting scheme = $1/[\sigma^2(F_o^2) + (0.0244P)^2]$ where $P = (F_o^2 + 2F_c^2)/3$.

heat for the phase transition of $Cs_8Sn_{44}$ at 90 °C was determined by linear interpolation of the DTA data of the melting point of naphthalene and of indium.

**EDX Analyses:** These were performed with a JEOL 5900LV Scanning Electron Microscope.

**Supporting Information** (see footnote on the first page of this article): Selected image plate frames and Rietveld refinements are available.

## Acknowledgments

The authors wish to thank the RTN program of the European Union (EU-project Nr. HPRN-CT 2002–00193) for financial support. We also thank Dr. Annette Schier for reading the manuscript.

[1] a) J. S. Kasper, P. Hagenmuller, M. Pouchard, C. Cros, *Science* **1965**, *150*, 1713–1714; b) K. A. Kovnir, A. V. Shevelkov, *Russ. Chem. Rev.* **2004**, *73*, 923–938.
[2] a) G. Slack, *CRC Handbook of Thermoelectrics*, CRC Press, **1995**; b) B. Iversen, G. Nolas, G. Stucky, *J. Solid State Chem.* **2000**, *149*, 455–458.
[3] S. Bobev, S. Sevov, *J. Solid State Chem.* **2000**, *153*, 92–105.
[4] J. T. Zhao, J. Corbett, *Inorg. Chem.* **1994**, *33*, 5721–5726.
[5] a) G. S. Nolas, B. C. Chakoumakos, B. Mahieu, G. J. Long, T. J. R. Weakley, *Chem. Mater.* **2000**, *12*, 1947–1953; b) J. L. Cohn, G. Nolas, V. Fessatidis, T. H. Metcalf, G. Slack, *Phys. Rev. Lett.* **1999**, *82*, 779–782; c) F. Chen, K. L. Stokes, G. Nolas, *J. Phys. Chem. Solids* **2002**, *63*, 827–832.
[6] a) S. Srinath, J. Gass, D. J. Rebar, G. T. Woods, H. Srikanth, G. Nolas, *J. Appl. Phys.* **2006**, *99*, 08K902(3); b) S. Paschen, W. Carrillo-Carbera, A. Bentien, V. H. Tran, M. Baenitz, Yu. Grin, F. Steglich, *Phys. Rev. B* **2001**, *64*, 214404(11).
[7] a) H. Q. Yuan, F. M. Grosche, W. Carrillo-Carbera, V. Pacheco, G. Sparn, M. Baenitz, U. Schwarz, Yu. Grin, F. Steglich, *Phys. Rev. B* **2004**, *70*, 174512(6); b) S. Paschen, V. H. Tran, M. Baenitz, W. Carrillo-Carbera, Yu. Grin, F. Steglich, *Phys. Rev. B* **2002**, *65*, 134435(9).
[8] J. S. Tse, S. Desgreniers, Z. Li, M. R. Ferguson, Y. Kawazoe, *Phys. Rev. Lett.* **2002**, *89*, 195507(4).
[9] J. Gallmeier, H. Schäfer, A. Weiss, *Z. Naturforsch., Teil B* **1969**, *24*, 665–667.
[10] H.-G. von Schnering, *Nova Acta Leopoldina* **1985**, *59*, 168.
[11] Yu. Grin, L. Melekhov, K. Chuntonov, S. Yatsenko, *Kristallografiya* **1987**, *32*, 497–498.
[12] G. Miller in *Chemistry, Structure, and Bonding of Zintl Phases and Ions* (Eds.: S. Kauzlarich), VCH Publishers, **1996**.
[13] H.-G. von Schnering, R. Kröner, M. Baitinger, K. Peters, R. Nesper, Yu. Grin, *Z. Kristallogr. – New Cryst. Struct.* **2000**, *215*, 205–206.
[14] C. Myles, J. Dong, O. Sankey, *Phys. Rev. B* **2001**, *64*, 165202(11).
[15] L. Mollnitz, N. Blake, H. Metiu, *J. Chem. Phys.* **2002**, *117*, 1302–1312.
[16] F. Dubois, T. Fässler, *J. Am. Chem. Soc.* **2005**, *127*, 3264–3265.
[17] G. Frisch, C. Hoch, C. Röhr, P. Zönnchen, K. Becker, D. Niemeier, *Z. Anorg. Allg. Chem.* **2003**, *629*, 1661–1672.
[18] T. B. Massalski, H. Okamoto, P. R. Subramanian, L. Kacprzak, *Binary Alloy Phase Diagrams* 5th ed., ASM-International, Materials-Park, **2004**.
[19] unpublished results.
[20] M. M. Shatruk, K. A. Kovnir, M. Lindsjö, I. A. Presniakov, L. A. Kloo, A. Shevelkov, *J. Solid State Chem.* **2001**, *161*, 233–242.
[21] J. Duenner, A. Mewis, *Z. Anorg. Allg. Chem.* **1995**, *621*, 191–196.
[22] W. Carrilo-Carbera, S. Budnyk, Y. Prots, Yu. Grin, *Z. Anorg. Allg. Chem.* **2004**, *630*, 2267–2276.
[23] I. Barin, O. Knacke, *Thermochemical Properties of Inorganic Substances*, Springer-Verlag, Berlin, **1973**.
[24] M. Baitinger, Yu. Grin, H.-G. von Schnering, R. Kniep, *Z. Kristallogr. – New Cryst. Struct.* **1999**, *214*, 457–458.
[25] a) F. H. Herbstein, *Acta Crystallogr., Sect. B* **2006**, *62*, 341–383; b) A. R. West, *Solid State Chemistry and Its Applications*, John Wiley & Sons Ltd., **1984**.
[26] H. Wondratschek, U. Müller, *International Tables for Crystallography, Volume A1 (Symmetry Relations Between Space Groups)*, Kluwer Academic Publishers, **2004**.
[27] T. Roisnel, J. Rodriguez-Carvajal, *FULLPROF,* Version 3.20, France, **2005**.
[28] *X-Shape Program: Crystal Optimization for Numerical Absorption Corrections*, Version 2.04, STOE Darmstadt, **2004**.
[29] G. Sheldrick, *SHELX-97, Program for Crystal Structure Determination*, University of Göttingen, **1997**.

Received: April 16, 2007
Published Online: July 24, 2007

  